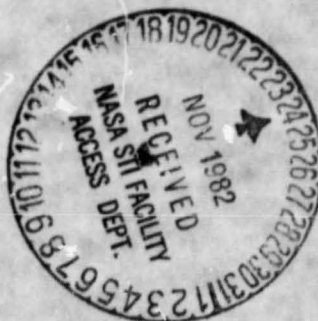# General Disclaimer

One or more of the Following Statements may affect this Document

- This document has been reproduced from the best copy furnished by the organizational source. It is being released in the interest of making available as much information as possible.

- This document may contain data, which exceeds the sheet parameters. It was furnished in this condition by the organizational source and is the best copy available.

- This document may contain tone-on-tone or color graphs, charts and/or pictures, which have been reproduced in black and white.

- This document is paginated as submitted by the original source.

- Portions of this document are not fully legible due to the historical nature of some of the material. However, it is the best reproduction available from the original submission.

Produced by the NASA Center for Aerospace Information (CASI)

Extended Performance 8-cm Mercury Ion Thruster

Maris A. Mantenieks
Lewis Research Center
Cleveland, Ohio

NASA

EXTENDED PERFORMANCE 8-cm MERCURY ION THRUSTER

Maris A. Mantenieks

National Aeronautics and Space Administration
Lewis Research Center
Cleveland, Ohio 44135

Abstract

A slightly modified 8-cm Hg ion thruster has demonstrated significant increases in performance. Thrust, for example, has been increased by almost a factor of five over that of the baseline thruster. Discussed in this paper are (1) thruster operation with various three grid ion optics configurations, (2) thruster performance as a function of accelerator grid open area, cathode baffle, and cathode orifice size, and (3) a life test of 614 hours at a beam current of 250 mA (17.5 mN thrust). Highest thruster efficiency was obtained with the smallest open area accelerator grid. The benefits in efficiency from the low neutral loss grids were mitigated, however, by the limitation such grids place on attainable ion beam current densities. The thruster components suffered negligible weight losses during the life test, which indicated that operation of the 8-cm thruster at extended levels of thrust and power is possible with no significant loss of lifetime.

Introduction

The 8-cm, 5.0-mN mercury ion thuster system was primarily developed to provide N-S station keeping of geosynchronous satellites with masses up to about 1800 kg. Recently, many missions have been proposed which employ satellites of much greater mass and area than present day concepts. Such Large Space Systems (LSS) include space based radars, large communications platforms, and space laboratories.[1,2] The on-orbit propulsion requirements of these large systems are beyond the capabilities of the present 8-cm thruster operated at baseline conditions. For example, for LSS with large area-to-mass ratios, solar pressure effect corrections become dominant[3,4] and greatly increase the requirements of on-orbit propulsion.

To satisfy these increased propulsion requirements, the thrust capability of the 8-cm thruster has been increased significantly over that of the baseline conditions.[5,6] This was accomplished by relatively minor mechanical modifications such as the addition of heat sinks for vaporizer thermal control and increasing the capability of the power supplies.

The objective of this study was to evaluate and optimize the 8-cm extended performance thruster with various other component changes including three-grid optics, variable baffle area, and cathode orifice size. Finally, thruster lifetime was evaluated while operating at high power and thrust levels (17.5 mN) by a life test of 614 hr.

Apparatus and Procedures

Thruster

The extended performance 8-cm thruster has been described in reference 5. Essentially, it is a SIT-8 thruster with heat sinks added to the vaporizer to allow vaporizer thermal control by prevention of thermal runaway over an increased range of discharge power. Three optics configurations which used three grids were evaluated with the extended performance thruster in this study and are described in Table 1. The screen and accelerator grid thicknesses of grid sets 1 and 2 were the same as those of the baseline two-grid 8-cm thruster. Grid set 3 consisted of three equally thick (0.25 mm (10 mils)) grids. The screen grid hole sizes were the same for all three configurations. The accelerator hole sizes ranged from 1.02 mm (40 mils) to 1.40 mm (55 mils), while the decelerator hole sizes varied from 1.52 mm (60 mils) to 1.90 mm (75 mils). All three configurations with the three grids were dished out with respect to the discharge chamber as opposed to the baseline thruster two-grid optics which were dished toward the discharge chamber.

The compensations of 0, 0.3, and 0.6 percent for the decelerator, accelerator and screen grids, respectively, were chosen rather arbitrarily and do not necessarily represent an optimum choice. The decelerator grid was operated at neutralizer potential.

For comparison, the thruster was also operated with the conventional two grid-geometry. The thruster performance was evaluated as a function of baffle area with two cathode orifice diameters of 0.25 mm (baseline design) and 0.73 mm.

Power Supplies and Vacuum Facility

The same power supplies and vacuum facility were used as in the previous study.[5] The output current of the discharge and screen grid supplies was limited to 4.5 and 1.0 A, respectively, and the screen grid voltage was limited to 2000 V. All tests, including the life test, were conducted in a 1.5 by 6.1-m vacuum facility operating at a pressure of about 1.3^{-4} Pa (1.0×10^{-6} torr). A no-load pressure of 4.0×10^{-5} Pa (3.0×10^{-7} torr) was usually attained in the facility.

Thruster Operation

The extended performance and baseline 8-cm thrusters operate with only one discharge chamber propellant flow-control loop. In the baseline 8-cm thruster, the control loop adjusts the vaporizer power to provide the correct flow rate to obtain a desired discharge voltage. The beam current is controlled by varying the discharge current at the desired discharge voltage. The baseline 8-cm thruster operates at a discharge current of 0.5 A, discharge voltage of 39 V, and a beam current of 72 mA. Higher beam current levels were achieved with the extended performance thruster by operating the thruster at higher discharge currents and higher flow rates.[5,6] The operating ranges of the thruster parameters were limited by the vaporizer thermal control characteristics and the available power supply capabilities.

2

Results and Discussion

The results of tests conducted to evaluate the extended performance 8-cm mercury ion thruster operation at high discharge power with various three-grid ion optics are presented. Operation with three-grid optics is of interest because (1) it may provide the capability to operate the thruster at lower ratios of screen voltage-to-total accelerating voltage (or R ratio), thus increasing the available range of specific impulse and thrust-to-power ratio, (2) it leads to reduction of charge-exchange erosion of the accelerator grid which increases thruster life and reduces the amount of metal effluents,[7] and (3) it offers reduction of ion beam divergence.[7]

Ion Optics

Perveance. - The current carrying capability, or perveance, of ion optics may be evaluated by measuring the accelerator and, for the three-grid systems, the decelerator current as the total voltage is varied. Typical accelerator and decelerator currents, as a function of total voltage, at two discharge power levels are seen in Figure 1 for grid set 2. Both grid impingement currents were considerably less than 1.0 percent of the beam current for most total voltages. The decelerater current ratio, however, approached the 1.0 percent level at high total voltages and low beam currents.

Another way of evaluating the current carrying capacity of a grid set is to plot the impingement current of both grids as a function of beam current at constant total voltage as shown in Figures 2 to 4. The impingement currents were measured for various discharge currents as the beam current was increased by increasing the mass flow rate. The steep increase of impingement current at high values of mass flow for each discharge current value was due to the increase in charge-exchange current as the mass utilization experienced a sudden decrease.

The accelerator impingement current-to-beam current ratio characteristics (Figs. 2(a), 3(a), 4(a)) were generally the same for all three-grid configurations. The baseline accelerator-to-beam current ratio was about 0.2 percent, with somewhat higher values at the low and high beam current values.

On the other hand, the decelerator to beam current ratio characteristics (Figs. 2(b), 3(b), 4(b)) showed a greater variation between grid sets. The decelerator-to-beam current ratio of grid set 1 (Fig. 2(b)) was large at low beam current levels and decreased to a baseline value of about 0.2 percent at a beam current level of about 250 mA. Lower ratios at low beam current levels were measured with grid set 2 (Fig. 3b). Baseline decelerator impingement characteristics similiar to those seen in Figure 3(b) were found by Aston[8] in studying grids with very limited numbers (19) of holes. In that study, high decelerator impingement currents at low perveance levels were shown to be a result of the divergence of high energy ions. Data from grid set 3, however, indicate that the observed high decelerator impingement currents can be alleviated somewhat by operating with thinner grids. As Figure 4(b) shows, decelerator impingement baseline current-to-beam current ratios were below 0.3 percent for most beam current values where the mass utilization was not very low. These low values were attained with a decelerator hole size of only 1.52 mm (60 mils), the same diameter as that of grid set 1 which experienced

3

large impingement currents (Fig. 2(b)). The results of this study indicate that three-grid operation is viable over a wide range of beam currents given proper selection of grid-hole diameter, compensation, grid gap, and grid thickness.

The perveance limits of the three accelerator screen-grid systems derived from data such as seen in Figure 1 are shown in Figure 5. Grid set 2, with the highest open area grid, exhibited the highest perveance. The perveance decreased almost linearly with decreasing open area of the accelerator grids. The expected increase of perveance with the decreased grid thickness of grid set 3 did not occur. The reason for this is not known at present.

The functional dependence of the current density on the total voltage, as indicated by the slopes of the curves in Figure 5, was about the same for all the three-grid sets tested. The slopes of 1.8 to 1.9 on Figure 5 are very close to the exponential value of 2.0 for the total voltage (V_T) found for the beam current $(J_b)_{max}$ carrying limit of a 30-cm thruster.[9]

$$(J_B)_{max} \cong \frac{1.7 \times 10^{-6} V_T^2}{1^2} \qquad (1)$$

where

$(J_B)_{max}$ maximum beam current, A
V_T total accelerating voltage, V
1 effective accelerating distance, mm

This expression was obtained by correlating a large quantity of data from many different geometries of dished grids of 30-cm mercury ion thrusters. The effective accelerating distance (1) was defined by Rawlin as the sum of the screen-grid thickness, the cold grid-to-grid spacing, three-fourths of the accelerator grid thickness, and change in the grid-to-grid spacing during thruster operation.

A noticeably different exponential value of 1.1 for V_T was measured using the conventional two-grid optics. The difference between the two-grid and three-grid behavior is thought to be due to the difference in the dishing direction of the grids because the dished-in and dished-out grids undergo an increase and a decrease, respectively, in grid-to-grid gap during thruster operation.

Ratio of the Net (Screen) to Total Voltage (R). Because of the interest in operating an 8-cm thruster over a wide range of specific impulse, tests were conducted over a range of screen-to-total voltage (R) ratios with all four grid configurations. Figure 6(a) shows the accelerator and decelerator impingement current of grid set 2 as a function of R for several beam currents at a constant total voltage of 2000 V. The accelerator current increased linearly with decreasing R until large-scale defocussing of the ion beam occured at an R value of about 0.2 for a beam current of 166 mA. At higher beam current levels, the onset of large-scale defocussing could not be reached because of recurring accelerator to screen voltage breakdowns. The reason for the breakdowns was not determined.

The decelerator impingment current-to-beam current ratio of grid set 2 was less than the accelerator-to-beam current ratio for all values of R

before the onset of large-scale ion impingement current. The minimum value of R ratio attained before the onset, as indicated in Figure 6(a), was about 0.2. The lowest R value of about 0.15 was reached with grid set 3 (Fig. 6(b)). Again, high-voltage breakdowns of grid set 3 prevented obtaining lower R ratios at higher beam currents. As indicated in Figure 6(c), the conventional two-grid set was also able to attain minimum R values as low as 0.2. Thus, in general, even with the encountered breakdown problems, minimum R values of 0.15 to 0.3 were obtained with all grids tested.

The ability to obtain minimum R values as low as 0.2 for the conventional two-grid optics differs from 30-cm grid behavior. It has been observed that 30-cm two-grid optics are limited to a minimum R value of about 0.5. The addition of the third grid has enabled the 30-cm optics to reach minimum R values of about 0.25.[9] The reason for the difference in performance between the 8- and 30-cm optics is not known at present.

In summary, the three-grid set with the highest accelerator open area (set 2) offered the highest perveance and low impingement current levels over a wide range of beam currents. The grid set with the lowest accelerator open area (set 1) had the lowest perveance and high decelerator impingement currents. The grid optics with the thin grids (set 3) allowed the lowest attainable R ratios and experienced low accelerator and decelerator impingement currents over the range of beam currents tested. Measured minimum R ratios of 0.15 to 0.3 for all 8-cm grid sets tested were somewhat lower than those obtained for the 30-cm three-grid optics operation.

Thruster Performance

Accelerator Open Area. The maximum beam currents of the extended 8-cm thruster as a function of the discharge power for the various three-grid optics are shown in Figure 7(a). The lowest power-per-beam ampere was obtained with the smallest open area accelerator grid (set 1), while a somewhat lower performance was achieved with grid sets 2 and 3. Figure 7(b) shows the mass utilization of the lowest (set 1) and the highest (set 2) open area accelerator grids as a function of beam current. As expected, the mass utilization with the lowest open area grid was consistently higher than the higher open area grids for all beam current values. The mass utilization of grid set 3 (not shown in Fig. 7(b)) was between the values of grid sets 1 and 2. A calculation of the effective open area, considering the effect of grid thickness, indicated that the difference of the thickness of grid 3 with respect to the other grids should not have a significant effect on mass utilization.

Cathode Orifice and Baffle Size. It was demonstrated previously[5] that thruster operation with a large cathode orifice diameter reduced the power-per-beam ampere at high beam currents at the expense of decreased mass utilization. This effect was pursued further in the present study. In order to obtain optimum thruster performance with the larger cathode orifice, tests were conducted to find an optimum baffle size for each accelerator open area configuration.

The effect of various baffle sizes on the maximum attainable beam current at a given discharge current is shown in Figure 8. Data are shown for both cathode sizes with the highest (set 2) and lowest (set 1) open area accelerator grids. The figure indicates that maximum beam current is

5

obtained for each configuration (i.e., cathode diameter and accelerator open area) with a different baffle diameter.

Figure 9 shows the comparison between the small orifice cathode and the large orifice cathode tests with the optimum baffle size. The data indicate that the power-per-beam ampere, at a given discharge power, is improved at the high beam current range with the large orifice cathode. Similar improvement with the larger orifice cathode was noted for grid set 3, for which the baffle size was not optimized. This may be seen in Figure 10, where the minimum power-per-beam ampere is plotted as a function of beam current. Improved performance with the large orifice cathode is apparent over the range of beam currents tested.

Figure 11 presents the mass utilization of the highest (set 2) and lowest (set 1) open area grids with the optimum size baffles. The smallest open area grid (set 1) still exhibited the highest mass utilization with the larger orifice cathode. Similarly, the small orifice cathode test with the highest open area grid (set 2) resulted in higher performance than with the large orifice size.

In summary, the larger orifice size offered lower power-per-beam ampere at the high beam current levels, but at some sacrifice of mass utilization. Also, highest performance was obtained by the lowest open area grids. However, as indicated before, the lowest open area configuration experienced large decelerator impingement currents. A compromise between the high current carrying capacity of grid set 2 and low neutral loss of grid set 1 may be the choice of the thin grid optics set 3. This grid configuration was found to have the lowest attainable R ratio, low impingement current levels and satisfactory mass utilization and power per beam ampere costs.

Overall Performance. The performance of the various thruster configurations tested may also be compared in Figure 12 where the total thruster efficiency is plotted as a function of thruster input power. A divergence loss factor of 0.95 and zero-double ion content were assumed. The last assumption was adopted because of the low discharge voltages experienced during high discharge power operation. Figure 12 was obtained by plotting the maximum efficiencies as the beam current was increased by increasing the flow rate at a given discharge current. The maximum efficiency did not correspond to the maximum attainable beam current at a given discharge power level because at that point, the mass utilization was not at its maximum value. Again, the least open area accelerator grid (set 1) showed the highest (70 to 80 percent) total thruster efficiencies, followed by increasing accelerator hole diameter sets 2 and 3. The large orifice cathode tests, because of the lower mass utilization, had considerably lower thruster efficiencies than the small orifice cathode tests. The general decrease of the total thruster efficiency with increasing input power is due to the increasing power per beam ampere costs.

Figure 13 presents the thrust-to-power ratio as a function of specific impulse for grid sets 1 and 2. The data were obtained by keeping the total voltage constant (2000 V) and varying the R ratio. The maximum thrust-to-power ratios of 46 to 48 mN/kW were obtained in the specific impulse range of 1500 to 2000 sec. Because the thrust to power ratio varied with beam current, an exact comparison between thruster configurations becomes somewhat difficult. However, as Figure 13 indicates, the dependence of thrust-to-power ratio on beam current is not strong and can, therefore, be concluded that the maximum thrust-to-power ratio for

the highest (set 2) and lowest (set 1) open area accelerator grids is not significantly different.

The thrust-to-power ratio of the baseline 8-cm thruster is somewhat lower than the extended thruster performance because the fixed losses such as vaporizer and neutralizer power are a significant percentage of the total baseline thruster input power, whereas in the extended thruster operation this is not the case.

Life Test

To evaluate the lifetime of the extended performance thruster operating at high beam current, a life test of the thruster with three-grid optics was performed. In conducting a life test, facility background gases must not significantly impact the life test results.[11, 12]. Spectroscopic measurements taken in the test facility have indicated that a no-load pressure of 4.0 x 10^{-5}Pa (3.0 x 10^{-7} torr) and an operating pressure of 1.3 x 10^{-4}Pa (1.0 x 10^{-6} torr) should be sufficient to obtain reliable lifetime data.[5]. The thruster life test was operated at a beam current of 250 mA and a thrust of 17.5 mN, which is about 3.5 times that of the baseline 8-cm thruster. Measured mass utilization during the life test was about 83 percent. (The other operating parameters are listed in Table 2.) The test was terminated after 614 hours for reasons of economy.

The thruster, on post-test examination, appeared in excellent condition. The weight changes of various thruster components are listed in Table 3. The baffle and screen grid are thruster components which usually suffer the most sputtering damage. The baffle, during the life test, experienced no weight change. The pole piece, screen, and decelerator grids gained small amounts of weight; the accelerator grid was the only component to lose weight.

Profilometer measurements indicated a uniform profile across the screen grid, in contrast to the 30-cm grid measurements after life tests where erosion rates were maximum at the grid center.[14]

A surface sputtering rate may be calculated from the following equation:

$$\dot{t} = 373.8 \frac{A}{\rho} \sum_{K=1}^{n} \frac{i_k S_k}{k} \tag{2}$$

where

$\dot{t}$ erosion rate, nm/hr
A   atomic weight of target material, AMU
ρ density of target material, g/cm^3
k   charge of impinging ion, k = 1,2...
i_k ion current density of each charged state, mA/cm^2
S_k sputter yield of incident ion, atoms/ion.

7

Assuming a sputter yield of 1.3 x 10^{-4} atoms/ion[14], a centerline ion beam current density of 9.8 mA/cm^2, and a doubly to singly charged current ratio of 0.01 [6], the calculated sputtering rate at the life test conditions was about 5 nm/hr. The effect of the doubly charged ion fraction was found to be negligible. At the calculated rate, only about 3x10^3 nm would have been expected to sputter at the center of the screen grid during the life test. This small change in thickness was about the limit of sensitivity of the available measuring device. However, the calculated rate and the low indicated rate from the life test, as well as erosion monitor measurements of reference 6, indicate a thruster screen-grid lifetime in excess of 20000 hr. For comparison, the calculated sputtering rate of the baseline thruster is about 4 nm/hr, which is only slightly less than the indicated extended performance thruster erosion rate.

The slight weight gain experienced by the screen grid is thought to be due to condensed sputtered material from the accelerator grid. Such a deposit can be seen on the downstream side of the screen grid (Fig. 14(a)). The center of the upstream side of the screen grid has the usual appearance of a sputtered surface (Fig. 14(b)). The slight deposition on the downstream side of the screen grid somewhat compromises the sputter erosion rate measurement, but as already indicated, the low calculated sputtering rate appears consistent with the low measured rate. The weight loss experienced by the accelerator grid was due to the enlargement of the accelerator holes from the original 1.4 to 1.53 mm on the downstream side of the grid. On the upstream side only the outer holes were slightly enlarged to 1.43 mm. It should be noted that the dimensional changes represent operation over a total of about 915 hr during which the perveance limits and operation at low R values for short time periods were conducted.

A deposit was found on the downstream side of the accelerator grid and is shown in Figure 15(a). It was presumed to originate from facility back-sputtered material. The dark ring evident around each accelerator hole is believed to be a shadow formed by the decelerator grid shielding the grid from the back-sputtered material flux. A thin layer spalled from the interior of an accelerator grid (seen in Fig. 15(b)), indicates that erosion of the inside of the accelerator holes had stopped during the life test and accumulation of back-sputtered material had commenced.

The decelerator grid weight gain most likely was due to the deposition of back-sputtered material on the downstream side of the grid. As seen in Figure 16(a), some notching is evident at the outermost holes of the decelerator grid. This may possibly be eliminated by a improved grid compensation. A charge-exchange-like pattern was found on the center of the upstream side of the decelerator grid as seen in Fig. 16(b). The depth of the pattern was too small to determine accurately.

Examination of the cathode tip after the life test revealed no apparent erosion or damage and the measured cathode orifice diameter was the same before and after the test.

The life test demonstrated a long lifetime capability of the 8-cm extended performance thruster operating with three-grid optics. Charge-exchange erosion appeared to be reduced. The presence of back-sputtered facility material on the life test thruster has made the exact evaluation of the lifetime of thruster components somewhat uncertain. However, the excellent condition of the thruster after the life test, evidenced by the

small weight changes measured, indicated that operation of the extended performance 8-cm thruster at high values of thrust and power is possible with adequate lifetime in excess of 20000 hr.

Conclusions

An extended performance 8-cm thruster was evaluated and optimized with respect to three different three-grid optics configurations, baffle diameter, and cathode orifice size. Also, thruster component lifetimes were evaluated by a life test of 614 hours.

As expected, the perveance limits of the three-grid optics correlated rather closely with the accelerator open area. The grid set with the highest open area offered the highest perveance and low impingement current levels over a wide range of beam currents. The grid set with the lowest accelerator open area had the lowest perveance and experienced high decelerator impingment currents over most of the beam current range tested. The grid optics with thin grids were found to have the lowest attainable R ratio (0.15) and low accelerator and decelerator impingement currents over the whole range of beam currents tested. Minimum R ratios of 0.15 to 0.3 were attained by all grids tested, including the conventional two-grid optics despite recurrent high-voltage breakdown problems at low R values. It was concluded that three-grid operation is viable over a wide range of beam currents including low perveance levels if proper grid-hole diameter, compensation, grid gap, and grid thickness are selected.

A maximum beam current at a given discharge power was obtained for each thruster configuration (i.e., cathode diameter and accelerator open area) with a different baffle diameter. Increased cathode orifice diameter was found to decrease power-per-beam ampere cost at high beam current levels but at a considerable reduction of mass utilization.

Highest thruster total efficiencies were attained with the smallest open accelerator area grid. However, because of the limited perveance, high impingement current of the smallest open area grid set, and the low mass utilization of the highest open area grid set, the thin grid set may offer the most desirable compromise between thruster performance and perveance. Total thruster efficiencies between 65 and 70 percent were attained by all three grids tested with the small orifice cathode over a wide range of thruster input power. Highest thrust-to-power ratio of about 45 mN/kw was attained by the highest open accelerator grid set.

The thruster was in excellent condition after the 614-hr life test. No weight loss was suffered by either the baffle or the screen grid. Only the accelerator grid lost weight. No appreciable charge-exchange erosion was detected. The presence of back-sputtered material on the thruster made evaluation of the lifetime of thruster components somewhat uncertain, however, the condition of the thruster after the 614-hr lifetime indicated that operation of the extended performance 8-cm thruster at high values of thrust and power is possible with adequate lifetime.

References

1. Smith, W. and W. and lark, J. P., "Study of Electrical and Chemical Propulsion Systems for Auxiliary Propulsion of Large Space Systems," Boeing Aerospace Co., Seattle, WA, D180-25956-3-Vol-1, D180-2595-4-Vol-2, Nov. 1981. (NASA-CR-165502-Vol-1 & 2.)

2. Byers, D. C. , "Upper Stages Utilizing Electric Propulsion," NASA TM-81412, 1980.

3. Lovell, R.R. and O'Mally, T. A., "Station Keeping of High Power Communication Satellites," NASA TM X-2136, Nov. 1970.

4. Wessel, F. J., Mantenieks, M. A., and DiEsposti, R. S., "On-Orbit Propulsion Requirements and Performance Assesment of Ion Propulsion Subsystems for Future Geo Large Satellite Missions" AIAA Paper 82-1872, Nov. 1982, New Orleans.

5. Mantenieks, M. A., "Performance Capabilities of the 8 cm Mercury Ion Thruster," AIAA Paper 81-0754, Apr. 1981.

6. Wessel, F. J. Williamson W. S., Dulgeroff, C.R., "Extended Performance 8-cm Ion Thruster Operation." AIAA Paper 82-1955, Nov. 1982, New Orleans.

7. Meadows, G. A. and Free, B. A., "Effect of a Decel Electrode on Primary and Charge-Exchange Ion Trajectories," AIAA Paper 75-427, Mar. 1975.

8. Wilbur, P. J., "Mercury Ion Thruster Research - 1977," NASA CR-135317, Dec. 1977.

9. Rawlin, V. K. and Hawkins, C. E., "Increased Capabilities of the 30-cm Diameter Hg Ion Thruster," AIAA Paper 79-0910, May 1979.

10. Rawlin, V. K., "Sensitivity of 30-cm Mercury Bombardment Ion Thruster Characteristics to Accelerator Grid Design," AIAA Paper 78-668, Apr. 1978.

11. Rawlin, V.K. and Mantenieks, M. A., "Effect of Facility Background Gases on Internal Erosion of the 30-cm Hg Ion Thruster," AIAA Paper 78-665, Apr. 1978.

12. Mantenieks, M. A. and Rawlin, V. K., "Sputtering in Mercury Ion Thrusters" AIAA Paper 79-2061, Oct. 1979.

13. Mantenieks, M. A. and Rawlin, V. K., "Sputtering Phenomena of Discharge Chamber Components in 30-cm Diameter Hg Ion Thrusters," AIAA Paper 76-988, Nov. 1976.

14. Askerov, Sh. G. and Sena, L. A., "Cathode Sputtering of Metals by Slow Mercury Ions," Soviet Physics - Solid State, Vol. 11, No. 6, Dec. 1969, pp. 1288-1293.

Table 1. - Description of grids tested

Grid set #	Grid	Hole size, mm	Thickness, mm	Compensation, percent	Screen-accel. center line gap, mm	Accel.-decel. center line gap, mm
#1	Screen	1.9	0.38	0.6	0.66	0.66
	Accel.	1.02	.51	.3	----	----
	Decel.	1.52	.38	0	----	----
#2	Screen	1.9	0.38	0.6	0.61	0.81
	Accel.	1.40	.51	.3	----	----
	Decel.	1.9	.38	0	----	----
#3	Screen	1.9	0.25	0.6	0.61	0.66
	Accel.	1.14	.25	.33	----	----
	Decel.	1.52	.25	0	----	----
Two grid	Screen	1.9	0.38	0.611	0.61	----
	Accel.	.89	.51	----	----	----
		1.14	----	----	----	----

Table 2. - Life Test Conditions

Beam current, mA	250
Discharge voltage, V	28
Discharge current, A	4.0
Screen grid voltage, V	1300
Accelerator grid voltage, V	350
Decelerator grid voltage (neutralizer potential), V	-24
Mass utilization, percent	83
Cathode orifice diameter, mm	0.25

Table 3. – Thruster component weight changes in 614-hour life test

Component	Weight change, percent
Baffle	0
Pole piece	.01
Accelerator grid	−1.46
Screen grid	.28
Decelerator grid	.007
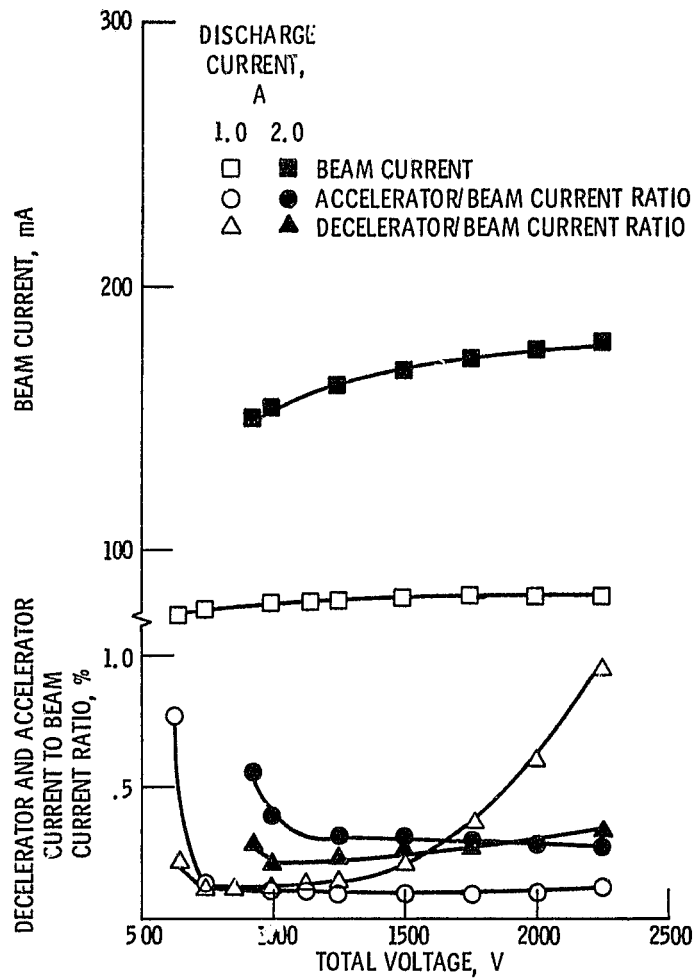
Figure 1. - Accelerator and decelerator current to beam
current ratio as a function of total voltage of a three-
grid set 2. R = 0.8; cathode orifice, 0.25 mm.

(a) Accelerator.
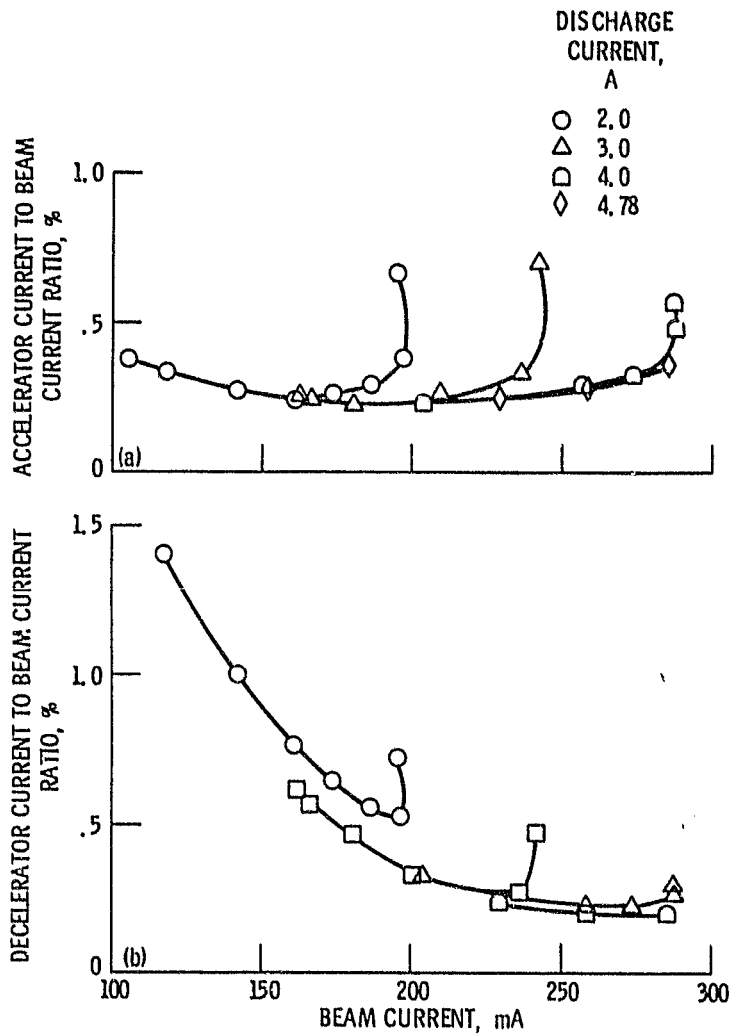
(b) Decelerator.

Figure 2. - Accelerator and decelerator current to beam current ratio as a function of beam current of three-grid set 1. R = 0.8; total voltage, 2000 V; cathode orifice, 0.25 mm.
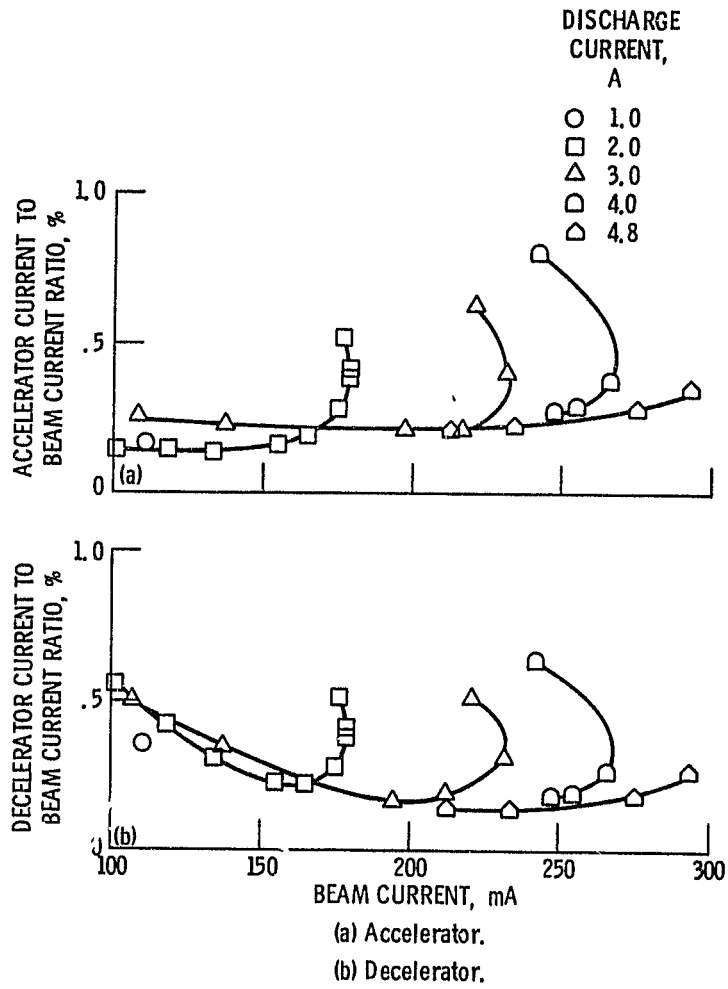
Figure 3. - Accelerator and decelerator current to beam current ratio as a function of beam current of three-grid set 2. R = 0.8; total voltage, 2000 V; cathode orifice, 0.25 mm.

(a) Accelerator.
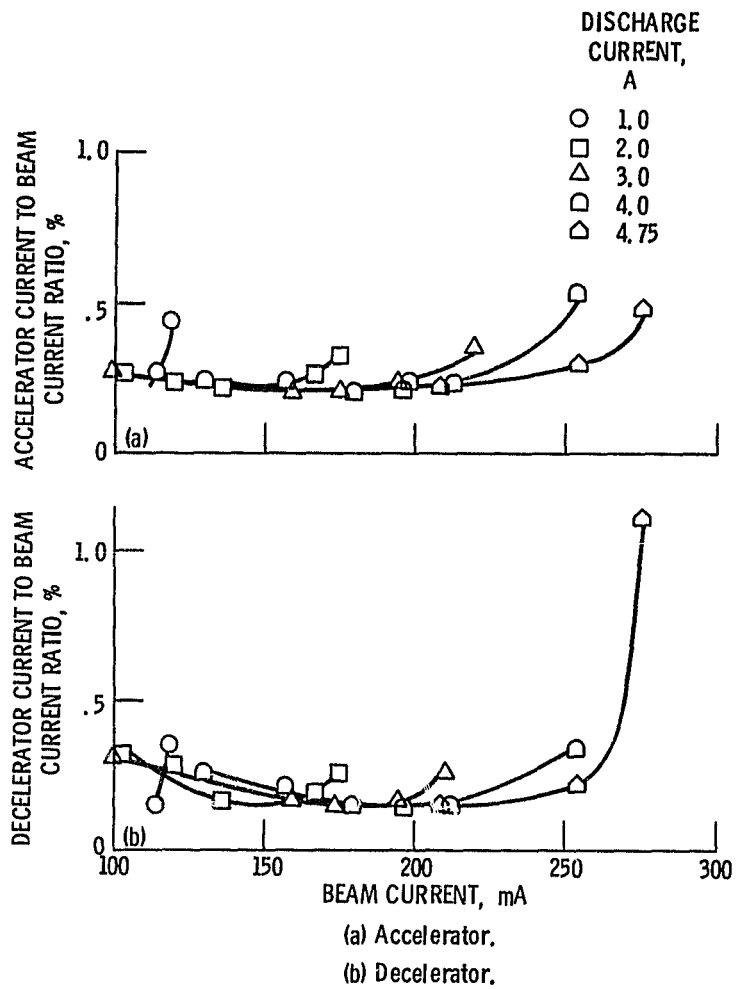
(b) Decelerator.

Figure 4. - Accelerator and decelerator current to beam current ratio as function of beam current of three-grid set 3. R = 0.8; total voltage, 2000 V; cathode orifice 0.25 mm.

	GRID SET	ACCELERATOR GRID OPEN AREA	PERVEANCE SLOPE
△	THREE-GRID 1	.26	1.9
◯	THREE-GRID 2	.49	1.8
◻	THREE-GRID 3	.33	1.8
◇	TWO-GRID	.27	1.1
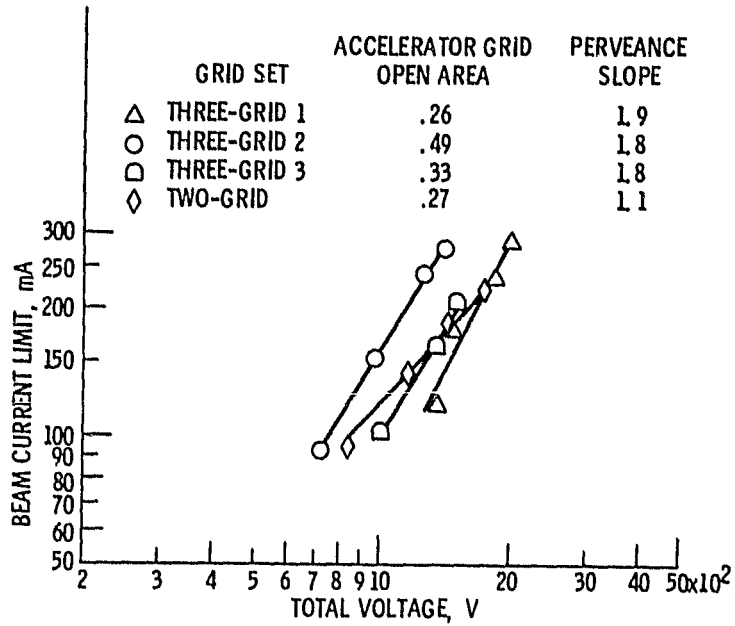
Figure 5. - Perveance comparisons of two and three-grid sets.
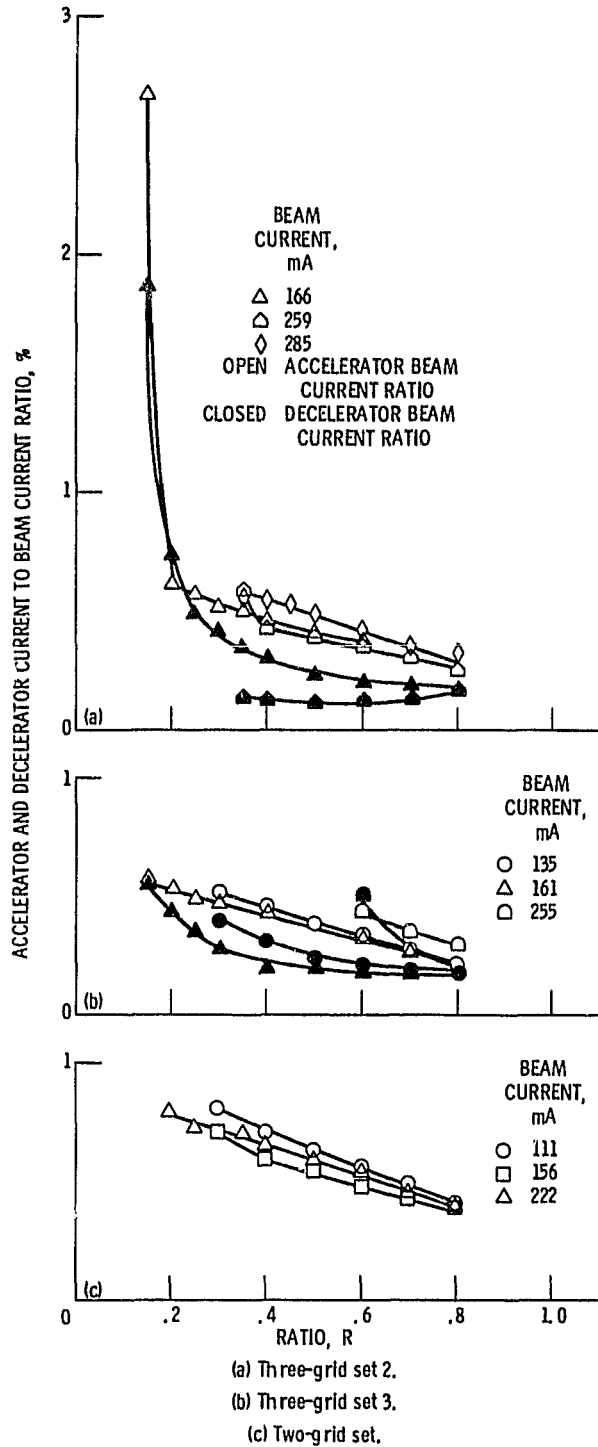
Figure 6. - Impingement current to beam current ratio as a
function of R ratio of various grid configurations. Total
voltage, 2000 V; cathode orifice, 0.25 mm.
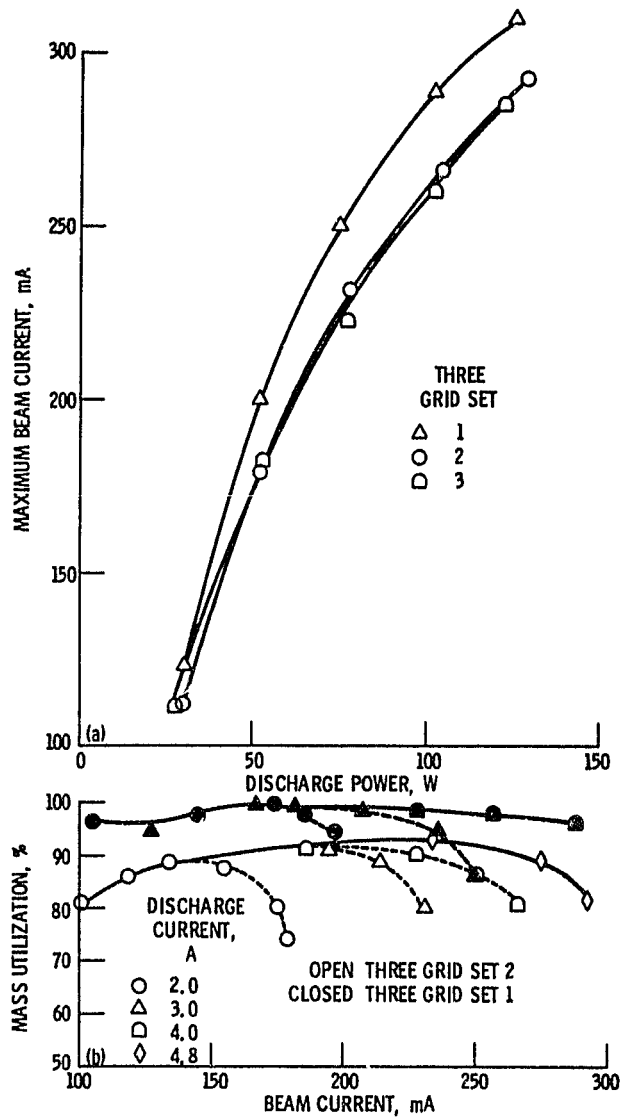
(a) Maximum attainable beam current as a function of discharge power.

(b) Mass utilization as function of beam current.

Figure 7. - Thruster performance with various three grid configurations. Total voltage, 2000 V; cathode orifice, 0.25 mm.
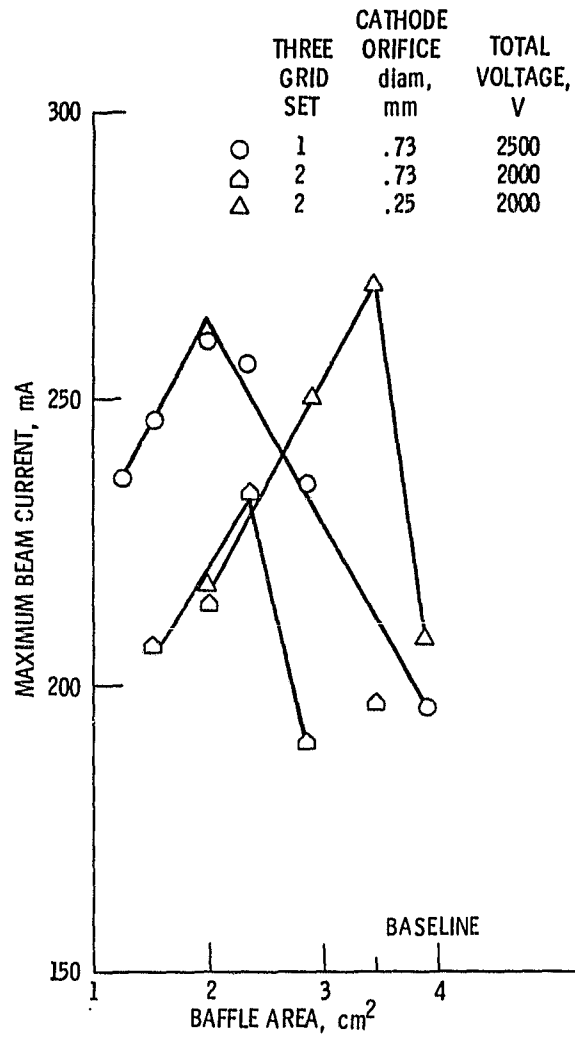
Figure 8. - Maximum beam current as function of baffle area for various accelerator grid and cathode orifice configurations. Discharge current, 3.0 A.
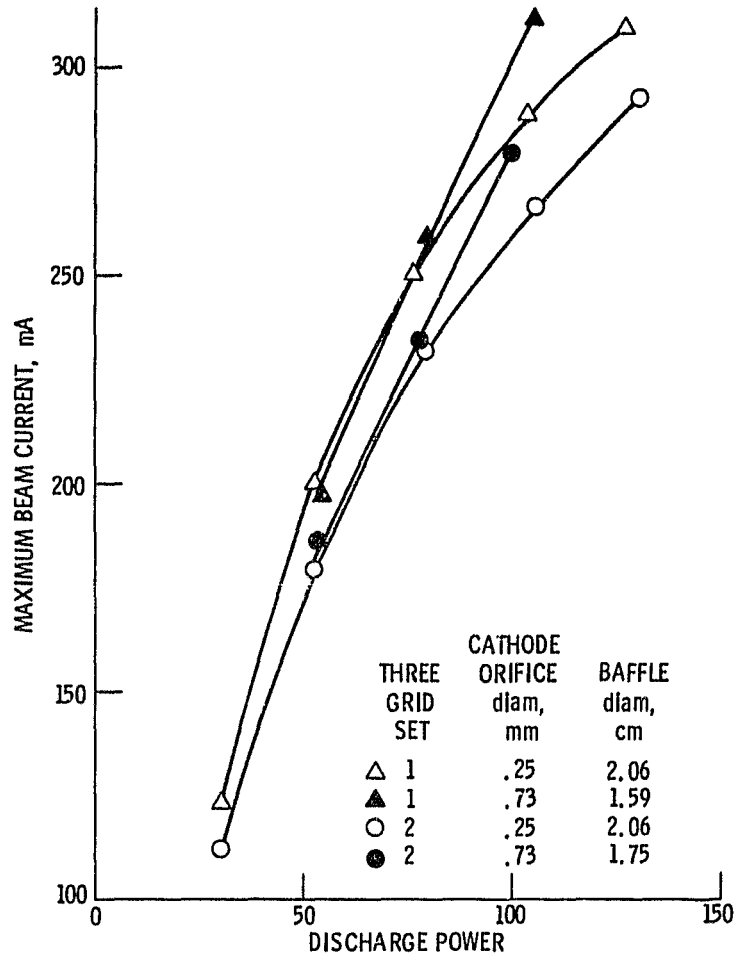
Figure 9. - Thruster performance as a function of discharge power for two cathode orifice diameters.
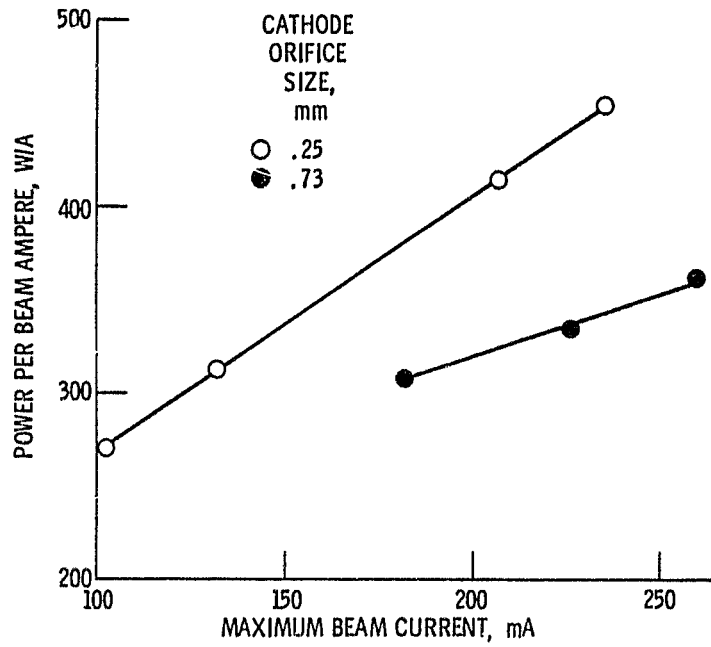
Figure 10. - Discharge power per beam ampere at a function of maximum beam current of three-grid set 3. Baffle diam, 2.06 cm.
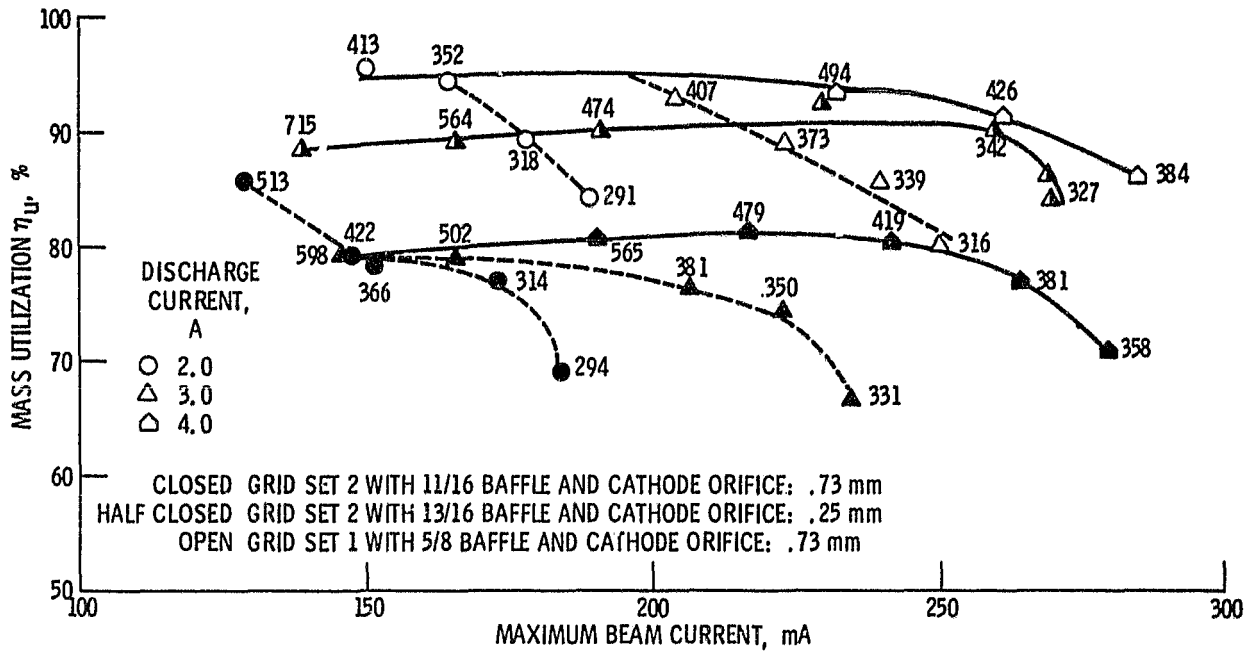
Figure 11. - Mass utilization as a function of beam current of three-grid sets 1 and 2 with optimized baffle sizes. Numbers denote power per beam ampere; total voltage, 2000 V.
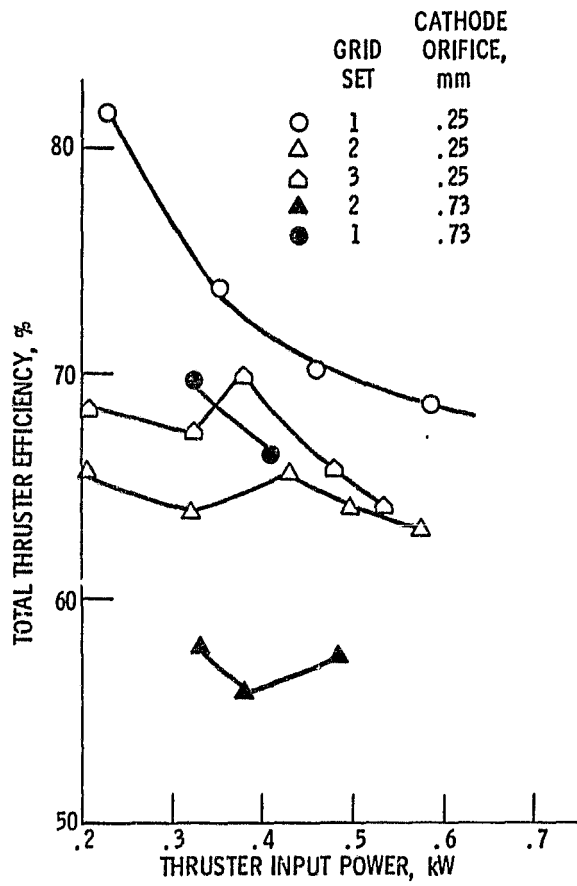
Figure 12. - Total thruster efficiency as a function of thruster input power for various configurations. Total voltage, 2000 V.
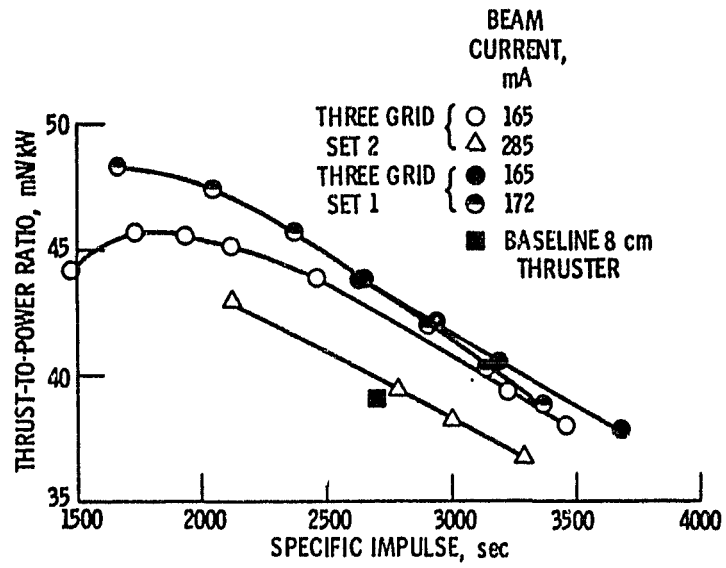
Figure 13. - Thrust to power ratio as a function of specific
impulse. Total voltage, 2000 V; cathode orifice, 0.25 mm.
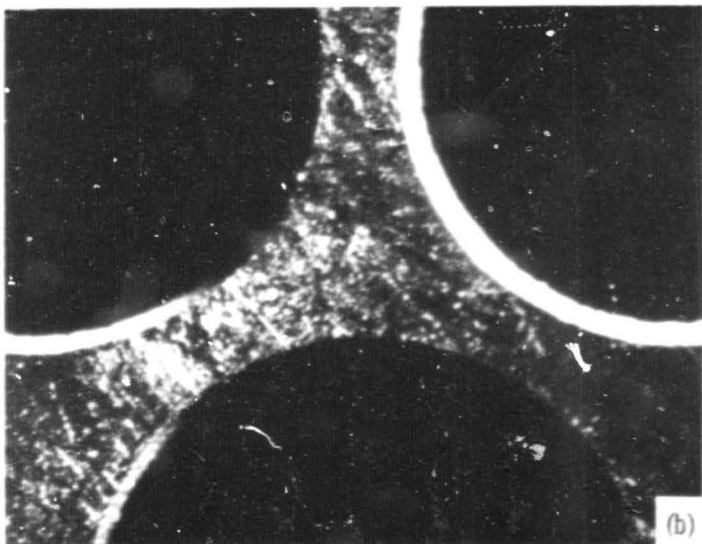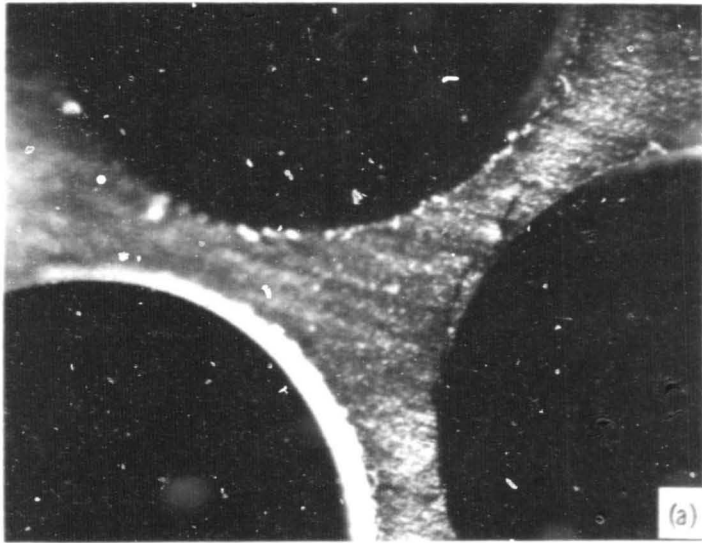
(a) Downstream side of screen grid (edge).
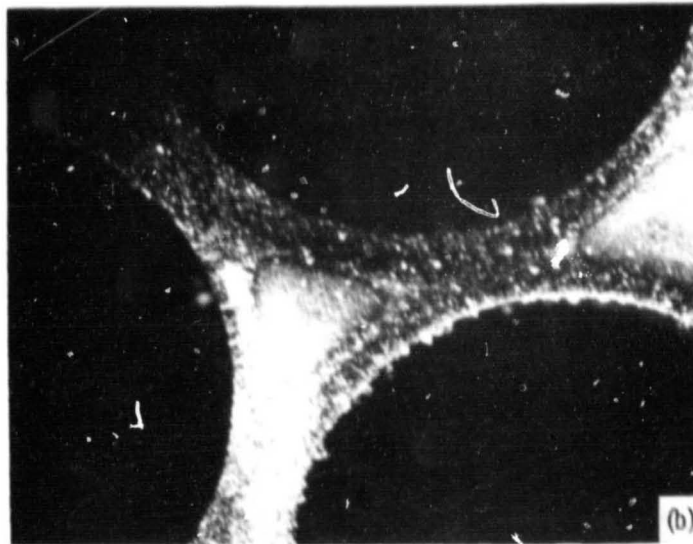
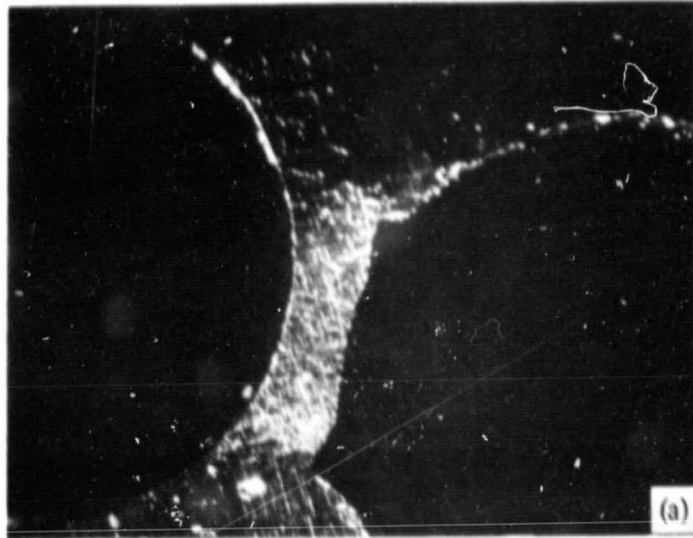(b) Upstream side of screen grid (center).

Figure 14. - Screen grid after 614 hr life test.
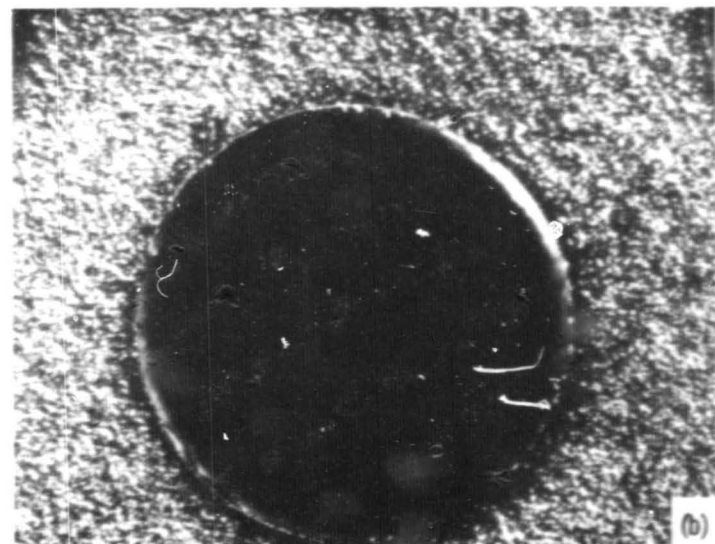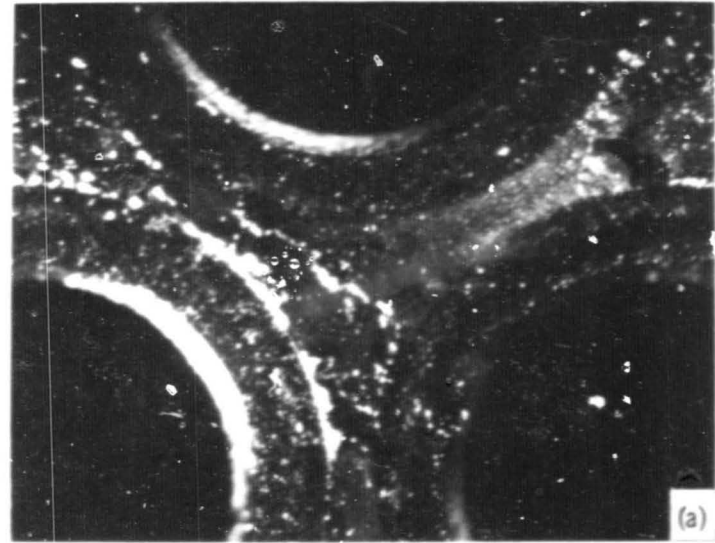
(a) Downstream side of accelerator (center).

(b) Upstream side of accelerator (center).

Figure 15. - Accelerator grid after 614 hr life test.

(a) Downstream side of decelerator (edge).

(b) Upstream side of decelerator (center).

Figure 16. - Decelerator grid after 614 hr life test.